

Modeling Spatial Smoothness in Fully 3-D SPECT Image Reconstruction Using Multiresolution B-Splines

Bryan W. Reutter, *Senior Member, IEEE*, Grant T. Gullberg, *Fellow, IEEE*, Arkadiusz Sitek, *Member, IEEE*, Rostyslav Boutchko, Elias H. Botvinick, and Ronald H. Huesman, *Fellow, IEEE*

Abstract—We investigated the use of B-spline spatial basis functions to model continuous 3-D tracer distributions in cardiac SPECT studies. This approach is motivated by goals of achieving a well-posed image reconstruction problem and computational efficiency. Uniform B-spline basis functions have the noteworthy property that splines having larger spatial support can be composed from a linear combination of splines having smaller support, thus facilitating creation of a multiresolution spatial model. B-splines can be evaluated quickly when calculating projection data models or displaying reconstructed images, and there is no image “blockiness” because B-splines yield a spatially continuous representation. We used trilinear B-splines to reconstruct images for a ^{99m}Tc -sestamibi cardiac SPECT/CT patient study. Attenuation and depth-dependent point response were modeled. Spline coefficients were estimated by minimizing a least-squares criterion by direct matrix inversion. Images were reconstructed with use of (1) more-spatially-compact splines, (2) less-spatially-compact splines, and (3) a multiresolution basis composed of more-compact splines in the heart volume and less-compact splines elsewhere. Image noise was reduced with use of less-compact or multiresolution splines, and the multiresolution basis also yielded good myocardial resolution. Encouraged by these results, we are using multiresolution B-splines to analyze dynamic SPECT data from rest/stress cardiac patient studies.

I. INTRODUCTION

WE investigated the use of multiresolution B-spline spatial basis functions to model continuous 3-D tracer distributions in cardiac single-photon emission computed tomography (SPECT) studies. This approach is motivated by goals of achieving a well-posed image reconstruction problem and computational efficiency. Use of splines and other “blob”-like basis functions in tomographic image reconstruction has

This work was supported by the National Heart, Lung, and Blood Institute of the U. S. Department of Health and Human Services under grants R01-HL50663 and R01-HL71253.

B. W. Reutter is with the Department of Functional Imaging, Lawrence Berkeley National Laboratory, University of California, Berkeley, CA 94720 USA (e-mail: bwreutter@lbl.gov).

G. T. Gullberg, R. Boutchko, and R. H. Huesman are with the Department of Functional Imaging, Lawrence Berkeley National Laboratory, University of California, Berkeley, CA 94720 USA.

A. Sitek was with the Department of Functional Imaging, Lawrence Berkeley National Laboratory, University of California, Berkeley, CA 94720 USA. He is now with the Department of Radiology, Brigham and Women’s Hospital & Harvard Medical School, Boston, MA 02115 USA.

E. H. Botvinick is with the Departments of Radiology & Medicine, University of California, San Francisco, CA 94143 USA.

been an active area of research (e.g., [1]–[3]), as has been use of multiresolution reconstruction grids (e.g., [4]).

Uniform B-spline basis functions can facilitate creation of a well-posed inverse problem by providing a spatially continuous, smooth representation of the image volume that is described by a relatively small number of parameters. Local spatial resolution (i.e., regularization) is specified explicitly by the design of the B-spline basis.

Uniform B-spline basis functions also have the noteworthy property that splines having larger spatial support can be composed from a linear combination of splines having smaller support, thus facilitating creation of a multiresolution spatial model. B-splines can be evaluated quickly when calculating projection data models or displaying reconstructed images, and there is no image “blockiness” because B-splines yield a spatially continuous representation.

We used trilinear B-splines to reconstruct images for a ^{99m}Tc -sestamibi cardiac SPECT/CT patient study. Attenuation and depth-dependent point response were modeled. Spline coefficients were estimated by minimizing a least-squares criterion by direct matrix inversion. Images were reconstructed with use of (1) more-spatially-compact splines, (2) less-spatially-compact splines, and (3) a multiresolution basis composed of more-compact splines in the heart volume and less-compact splines elsewhere. Image noise was reduced with use of less-compact or multiresolution splines, and the multiresolution basis also yielded good myocardial resolution.

II. PROPERTIES OF UNIFORM B-SPLINES

The k th-order uniform B-spline basis function, $\Pi^{*k}(x)$, is the piecewise $(k-1)$ st-degree polynomial that is obtained by convolving the rectangle function

$$\Pi(x) = \begin{cases} 1 & x \in [-\frac{1}{2}, \frac{1}{2}] \\ 0 & \text{otherwise} \end{cases} \quad (1)$$

with itself $k-1$ times (Fig. 1). The Gaussian is obtained in the limit as the order k approaches infinity. The function $\Pi^{*k}(x)$ has a support of width k , a standard deviation of $\sqrt{k/12}$, and unit integral (i.e., $\int_{-\infty}^{\infty} \Pi^{*k}(x)dx = 1$). A convenient analytical expression for the k th-order uniform B-spline basis function is

$$\Pi^{*k}(x) = \frac{1}{(k-1)!} \sum_{j=0}^k \binom{k}{j} (-1)^j \left[x + \frac{k}{2} - j \right]_+^{k-1} \quad (2)$$

where

$$[x - v]_+ = \begin{cases} 0 & x \in (-\infty, v) \\ x - v & x \in [v, \infty) \end{cases} \quad (3)$$

is the one-sided linear basis function [5].

The appropriately scaled function having a support of width ak , a standard deviation of $a\sqrt{k/12}$, and unit integral is $\frac{1}{a}\Pi^{*k}\left(\frac{x}{a}\right)$, for $a > 0$. The Fourier transform of $\frac{1}{a}\Pi^{*k}\left(\frac{x}{a}\right)$ is $\text{sinc}^k(as)$ (Fig. 2).

The support of the k th-order uniform B-spline basis function $\frac{1}{a}\Pi^{*k}\left(\frac{x}{a}\right)$ can be doubled (Fig. 3) simply by taking a linear combination of $k + 1$ shifted versions of itself [6]:

$$\frac{1}{2a}\Pi^{*k}\left(\frac{x}{2a}\right) = \frac{1}{2^k} \sum_{j=0}^k \binom{k}{j} \left[\frac{1}{a}\Pi^{*k}\left(\frac{x}{a} + \frac{k}{2} - j\right) \right]. \quad (4)$$

Thus, in tomographic imaging the forward-projection matrix for lower-resolution splines is just a linear combination of the columns of a matrix for higher-resolution splines.

III. $^{99\text{M}}\text{Tc}$ -SESTAMIBI CARDIAC SPECT/CT PATIENT STUDY

For computational simplicity, we used separable, trilinear B-splines [i.e., products of the form $\Pi^{*2}(x)\Pi^{*2}(y)\Pi^{*2}(z)$] to reconstruct images for a $^{99\text{M}}\text{Tc}$ -sestamibi cardiac SPECT/CT patient study.

A. SPECT/CT Data Acquisition

Data were acquired with use of parallel-hole collimators on a dual-head GE Millennium VH Hawkeye SPECT/CT scanner. A 30 min dynamic scan was performed, with the patient's arms down for comfort, subsequent to pharmacologically induced stress as part of a rest/stress protocol. During the dynamic scan, the gantry performed 24 360-degree rotations, acquiring 72 views per rotation at 1 sec per view. Projections at each view were binned into 64×64 frames, with a bin size of $8.84 \text{ mm} \times 8.84 \text{ mm}$. For purposes of this investigation, emission data acquired about 2–30 min post-injection (i.e., during the last 22 rotations) were summed to obtain a static dataset. Images were reconstructed from projections of the heart obtained in 64 (transverse) \times 9 (axial) sub-frames of the 72 views, which contained a total of about 6.8 million detected events (Fig. 4). An X-ray CT scan was performed with use of the integrated Hawkeye system to obtain an attenuation map (Fig. 5).

B. Higher-Resolution, Lower-Resolution, and Multiresolution B-Spline Image Space Models

A higher-resolution model for image space, based on more-spatially-compact B-splines, was obtained by first thresholding the attenuation map to obtain a mask for the patient's body and the bed. The volume encompassed by the mask was then spanned by 7659 overlapping trilinear B-splines organized on a $63 \times 63 \times 5$ rectangular grid having a spacing of $8.84 \text{ mm} \times 8.84 \text{ mm} \times 17.7 \text{ mm}$ along the x -, y -, and z -axes, respectively, where x and y are transverse coordinates and z is the axial

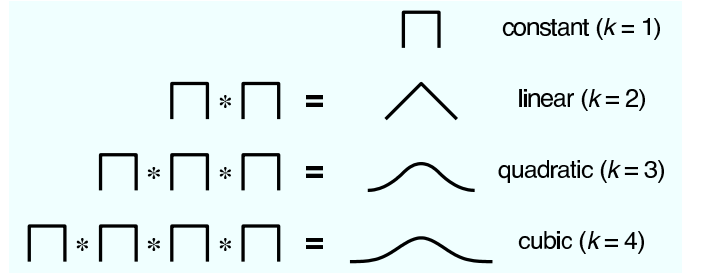


Fig. 1. The k th-order uniform B-spline is obtained by convolving the rectangle function with itself $k - 1$ times.

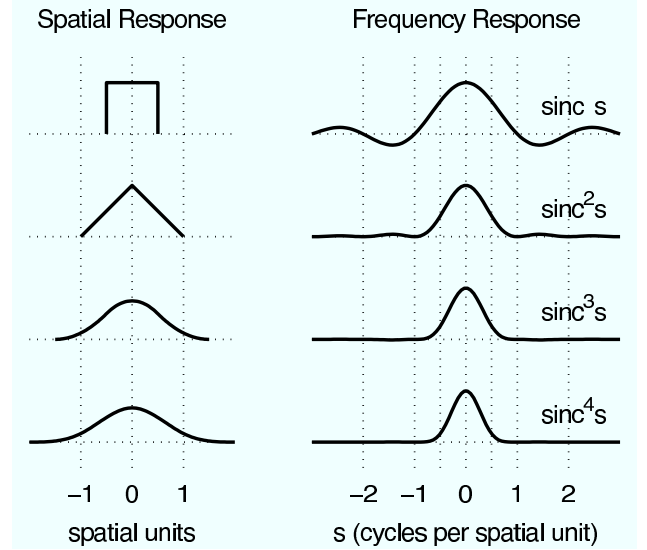


Fig. 2. Spatial frequency responses for 1-D uniform B-splines.

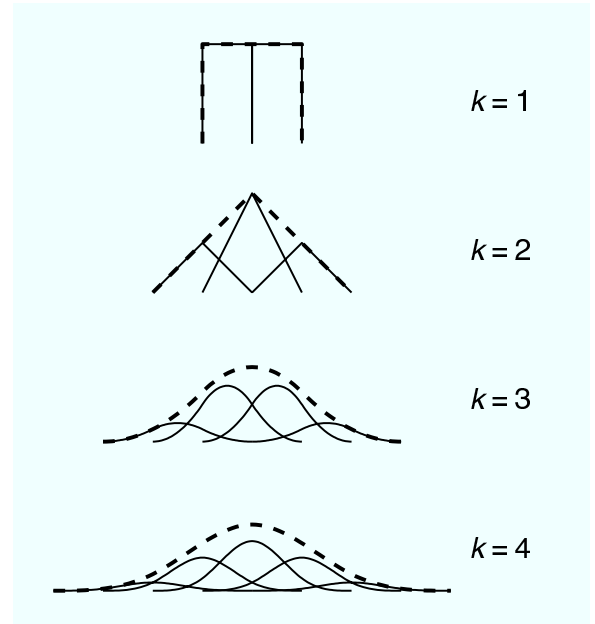


Fig. 3. Doubling the support of uniform B-splines via equation (4), in which $k + 1$ weighted and shifted versions of $\Pi^{*k}(x)$ (solid curves) are summed to obtain $\frac{1}{2}\Pi^{*k}\left(\frac{x}{2}\right)$ (dashed curves).

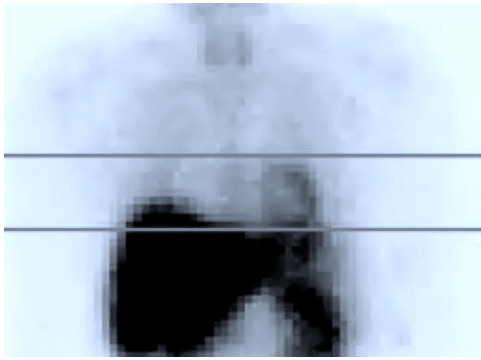


Fig. 4. Anterior view of summed late projection data from a ^{99m}Tc -sestamibi cardiac SPECT patient study. The volume between the gray lines was reconstructed.

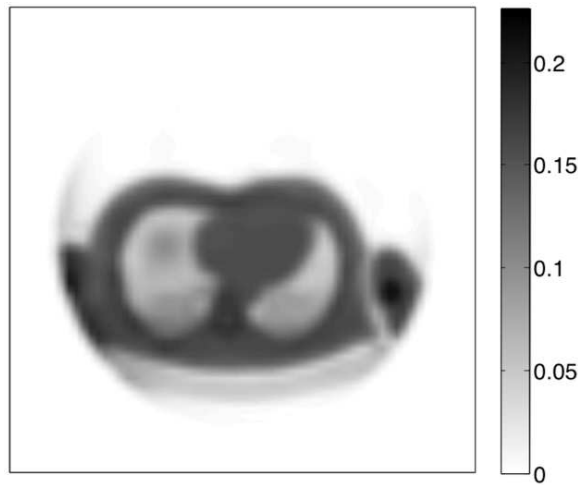


Fig. 5. Smoothed attenuation map for a transverse mid-ventricular slice acquired by the integrated Hawkeye X-ray CT system.

coordinate. The overlapping splines had a support of $17.7 \text{ mm} \times 17.7 \text{ mm} \times 35.4 \text{ mm}$ along x , y , and z , respectively.

A lower-resolution spatial model based on less-spatially-compact B-splines was then obtained by doubling the transverse support of the higher-resolution splines (Fig. 3) and downsampling in the transverse plane. This yielded a total of 2201 overlapping trilinear B-splines organized on a $31 \times 31 \times 5$ rectangular grid having a spacing of $17.7 \text{ mm} \times 17.7 \text{ mm} \times 17.7 \text{ mm}$ along x , y , and z , respectively. The overlapping splines had a support of $35.4 \text{ mm} \times 35.4 \text{ mm} \times 35.4 \text{ mm}$ along x , y , and z , respectively.

Finally, a multiresolution spatial model was obtained by replacing a $6 \times 6 \times 5$ neighborhood of lower-resolution splines that spanned the heart volume with an $11 \times 11 \times 5$ neighborhood of higher-resolution splines, to obtain a total of 2626 spatial basis functions (Fig. 6). Fig. 7 shows the multiresolution SPECT image reconstructed for the transverse mid-ventricular slice corresponding to Fig. 5 (details of the reconstruction methods and additional results follow).

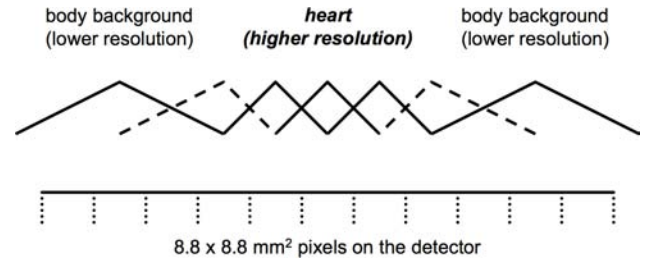


Fig. 6. Depiction of spatial scales for higher- and lower-resolution components of multiresolution trilinear B-spline basis functions, relative to the SPECT detector bins. Dashed lines indicate splines that provide a smooth transition between higher- and lower-resolution components.

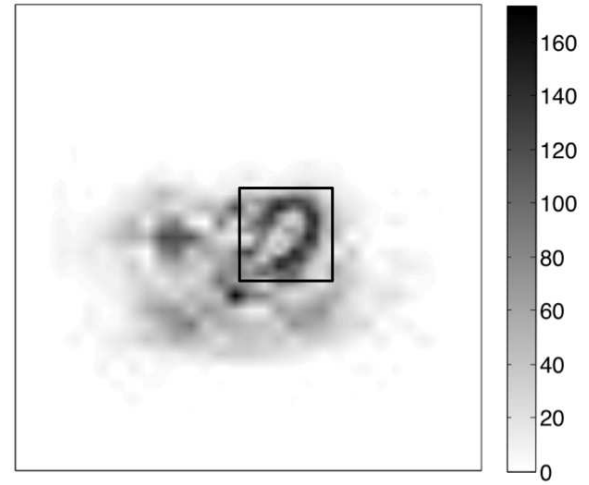


Fig. 7. Multiresolution SPECT image reconstructed for the transverse mid-ventricular slice corresponding to Fig. 5. The box outlines the higher-resolution component of the image.

C. Projection Data Models, Least-Squares Minimization, and Reconstructed Images

For the higher-resolution spatial basis, a system model that related spatial spline intensities to detected events was calculated with use of a ray-driven projector [7] that modeled depth-dependent collimator response, as well as attenuation based on the measured attenuation map. Scatter was not modeled. This resulted in a projection data model $\mathbf{F}\mathbf{a} = \mathbf{p}$, where \mathbf{F} is a 34472×7659 system matrix, \mathbf{a} is a 7659-element column vector of spline coefficients, and \mathbf{p} is a 34472-element column vector of modeled projection values. An estimate, $\hat{\mathbf{a}}$, of spatial spline coefficients was obtained by minimizing the sum of squared differences between the measured projections, \mathbf{p}^* , and the modeled projections. The least-squares solution, given by $\hat{\mathbf{a}} = (\mathbf{F}^T \mathbf{F})^{-1} \mathbf{F}^T \mathbf{p}^*$, was obtained by directly inverting the 7659×7659 matrix $\mathbf{F}^T \mathbf{F}$, where the superscript "T" denotes the matrix transpose. Using a dual 2.5 GHz PowerPC G5 Macintosh and MATLAB software, the matrix inversion took about 2.9 min. Post-reconstruction smoothing was performed in the transverse plane with a separable 3×3 filter that smoothed spline coefficients with a $[1/4 \ 1/2 \ 1/4]$ kernel first along the x -

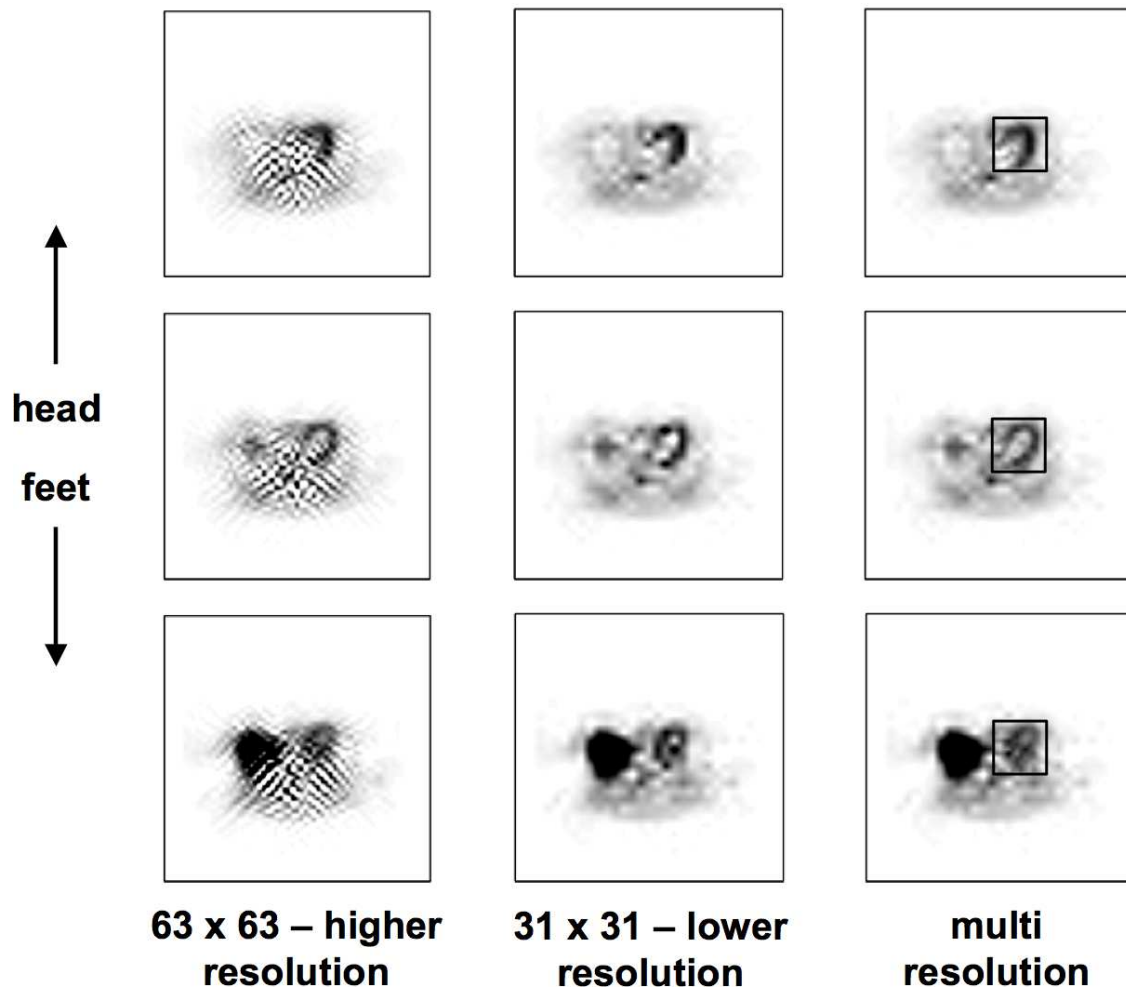


Fig. 8. Reconstructed SPECT images for three transverse slices of a ^{99m}Tc -sestamibi cardiac SPECT/CT patient study. The middle row corresponds to the mid-ventricular slice shown in Figs. 5 and 7. The left and middle columns show images obtained with use of higher-resolution and lower-resolution B-splines, respectively. The right column shows images obtained with use of a multiresolution basis that has higher resolution in the heart volume (outlined by boxes) and lower resolution elsewhere in the body. The colormap for all images is the same as that for Fig. 7.

axis and then along the y -axis. The left columns of Figs. 8 and 9 show the reconstructed images. Excessive noise and artifacts are evident and are probably due to having only 72 angular samples and 64 lateral samples [8].

For the lower-resolution spatial basis, the 2201 columns of the system matrix \mathbf{F} were obtained by taking linear combinations of the columns of the system matrix for the higher-resolution basis. Inversion of 2201×2201 matrix $\mathbf{F}^T \mathbf{F}$ took only about 5 sec. No post-reconstruction smoothing was performed. The middle columns of Figs. 8 and 9 show the reconstructed images, which have reduced noise and artifacts compared to the higher-resolution images.

For the multiresolution spatial basis, the 2626 columns of the system matrix \mathbf{F} were obtained by replacing 180 columns (corresponding to a $6 \times 6 \times 5$ array of lower-resolution splines spanning the heart volume) of the lower-resolution system matrix with 605 columns (corresponding to an $11 \times 11 \times 5$ array of higher-resolution splines) of the higher-resolution system

matrix. System matrix columns for higher-resolution splines adjacent to the boundary between higher and lower resolution were adjusted to provide a smooth transition (dashed lines in Fig. 6). Inversion of 2626×2626 matrix $\mathbf{F}^T \mathbf{F}$ took only about 8 sec. Post-reconstruction smoothing in the transverse plane was performed only on higher-resolution spline coefficients with a separable 3×3 filter that smoothed with a $[1/4 \ 1/2 \ 1/4]$ kernel first along the x -axis and then along the y -axis. The right columns of Figs. 8 and 9 show the reconstructed images, which have reduced noise and artifacts compared to the higher-resolution images and better myocardial resolution than the lower-resolution images.

IV. FUTURE DIRECTIONS

Encouraged by these results, we are using multiresolution spatial B-splines to analyze dynamic SPECT data from rest/stress cardiac patient studies using methods similar to those which we reported in [9]–[11]. Future work includes implementation of spatial modeling with tri-quadratic B-splines, which

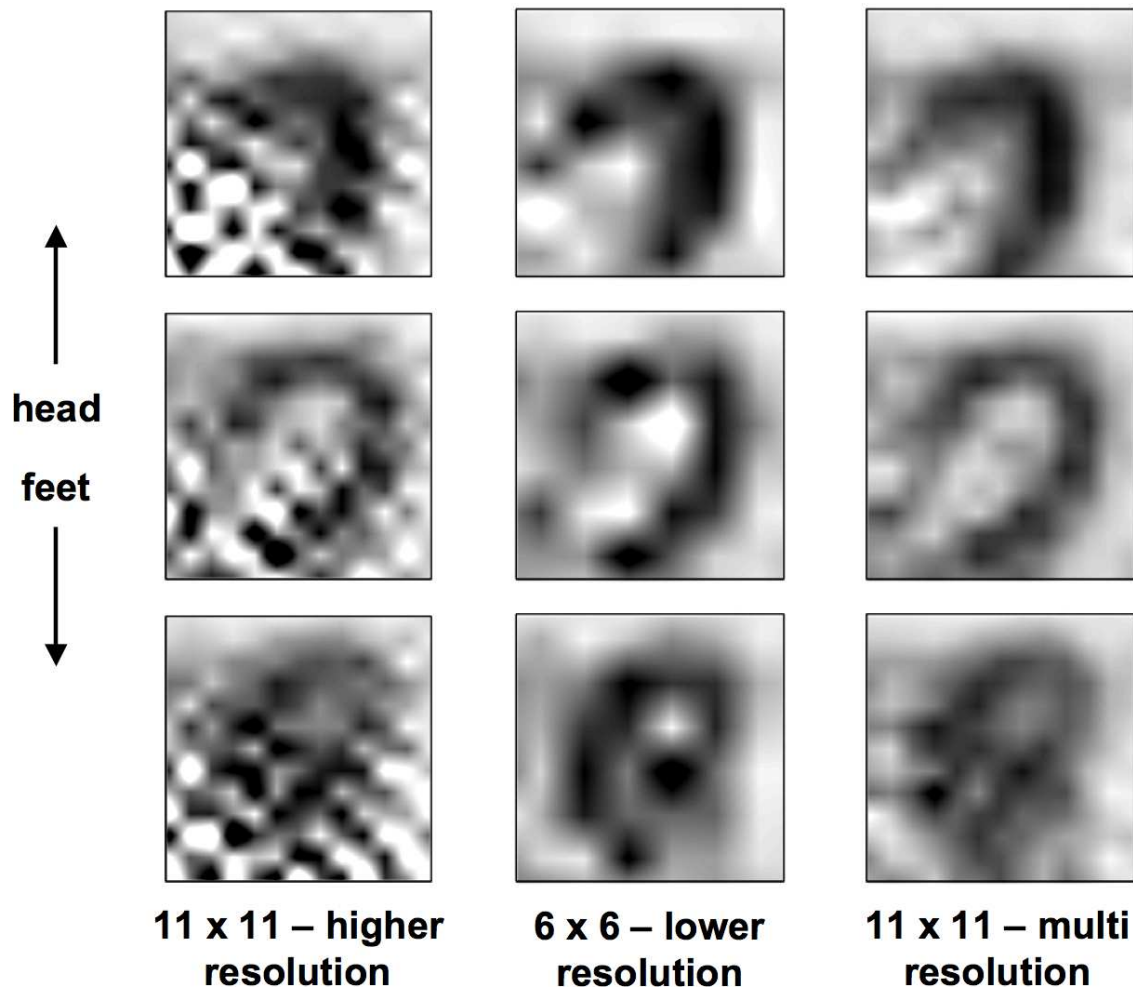


Fig. 9. Zoomed heart images for volume outlined by boxes in images in right column of Fig. 8. The colormap for all images is the same as that for Fig. 7.

are smoother and more circularly symmetric than trilinear B-splines. We are also investigating the use of spatial B-splines for reconstruction based on penalized weighted least-squares minimization or iterative maximization of Poisson likelihood.

ACKNOWLEDGMENT

This work was supported by the National Heart, Lung, and Blood Institute of the U. S. Department of Health and Human Services under grants R01-HL50663 and R01-HL71253.

REFERENCES

- [1] R. M. Lewitt, "Multidimensional digital image representations using generalized Kaiser-Bessel window functions," *J Opt Soc Am A*, vol. 7, no. 10, pp. 1834–1846, 1990.
- [2] S. Horbelt, M. Liebling, and M. Unser, "Discretization of the Radon transform and of its inverse by spline convolutions," *IEEE Trans Med Imag*, vol. 21, no. 4, pp. 363–376, 2002.
- [3] A. Yendiki and J. A. Fessler, "A comparison of rotation- and blob-based system models for 3D SPECT with depth-dependent point response," *Phys Med Biol*, vol. 49, no. 11, pp. 2157–2168, 2004.
- [4] J. S. Maltz, "Optimal time-activity basis selection for exponential spectral analysis: Application to the solution of large dynamic emission tomographic reconstruction problems," *IEEE Trans Nucl Sci*, vol. 48, no. 3, pp. 1452–1464, 2001.
- [5] R. H. Bartels, J. C. Beatty, and B. A. Barsky, *An Introduction to Splines for Use in Computer Graphics and Geometric Modeling*. Los Altos, CA: Morgan Kaufmann, 1987.
- [6] M. Unser, "Splines: A perfect fit for signal and image processing," *IEEE Signal Processing Magazine*, vol. 16, no. 6, pp. 22–38, 1999.
- [7] G. L. Zeng, G. T. Gullberg, B. M. W. Tsui, and J. A. Terry, "Three-dimensional iterative reconstruction algorithms with attenuation and geometric point response correction," *IEEE Trans Nucl Sci*, vol. 38, no. 2, pp. 693–702, 1991.
- [8] R. H. Huesman, "The effects of a finite number of projection angles and finite lateral sampling of projections on the propagation of statistical errors in transverse section reconstruction," *Phys Med Biol*, vol. 22, no. 3, pp. 511–521, 1977.
- [9] B. W. Reutter, G. T. Gullberg, and R. H. Huesman, "Kinetic parameter estimation from dynamic cardiac patient SPECT projection measurements," in *1998 IEEE Nuclear Science Symposium and Medical Imaging Conference Record*, R. Sudharsanan, Ed., 1999, pp. 1953–1958.
- [10] —, "Direct least-squares estimation of spatiotemporal distributions from dynamic SPECT projections using a spatial segmentation and temporal B-splines," *IEEE Trans Med Imag*, vol. 19, no. 5, pp. 434–450, 2000.
- [11] B. W. Reutter, S. Oh, G. T. Gullberg, and R. H. Huesman, "Improved quantitation of dynamic SPECT via fully 4-D joint estimation of compartmental models and blood input function directly from projections," in *2005 IEEE Nuclear Science Symposium and Medical Imaging Conference Record*, B. Yu, Ed., 2005, pp. 2337–2341.